Canadian Science Publishing

ARTICLE

Modelling short-term monotonic response of timber–concrete composite structures

Cong Liu, Anca C. Ferche, and Frank J. Vecchio

Abstract: Timber–concrete composite is an efficient hybrid construction material that exploits the advantageous properties of timber and concrete. The use of shear connectors enables the two dissimilar materials to act together, resulting in an increase in global stiffness as well as load-carrying capacity. As this composite material is becoming increasingly more popular in the construction industry, there is a need to develop analysis tools that have general applicability to timber–concrete composite systems with variations in loading schemes, specimen configurations, materials, and types of shear connectors. One such tool, a generic two-dimensional nonlinear finite element model, is proposed in this paper; it is verified through numerical simulations of six experiment series carried out by other researchers. Good agreement between experimentally observed behaviour and numerical simulations was generally obtained.

Key words: timber–concrete composite, shear connectors, structures, modelling, finite element analysis.

Résumé : Le composite bois–béton est un matériau de construction hybride efficace qui exploite les propriétés avantageuses du bois et du béton. L'utilisation de connecteurs de cisaillement permet aux deux matériaux dissemblables d'agir ensemble, entraînant une augmentation de la rigidité globale ainsi que de la portance. Comme ce matériau composite est de plus en plus populaire dans l'industrie de la construction, il est nécessaire de développer des outils d'analyse qui sont généralement applicables aux systèmes composites bois–béton avec des variations dans les schémas de chargement, les configurations de spécimens, les matériaux et les types de connecteurs de cisaillement. L'un de ces outils, un modèle des éléments finis non linéaires non bidimensionnels générique, est proposé dans cet article; il est vérifié par des simulations numériques de six séries d'expériences réalisées par d'autres chercheurs. On a généralement obtenu une bonne concordance entre le comportement observé expérimentalement et les simulations numériques. [Traduit par la Rédaction]

Mots-clés : composite bois–béton, connecteurs de cisaillement, structures, modélisation, analyse des éléments finis.

Introduction

Timber–concrete composite (TCC) systems have seen increased development in the past two decades, finding extensive structural applications, including renovation and upgrading of existing timber structures, new construction of mid- to low-rise buildings, and construction of mid- to short-span bridges (Yeoh et al. 2011; Ceccotti 2002; Le Roy et al. 2009). The composite system typically takes the form of a concrete slab supported by timber beams or panels. Thus, the advantageous properties of both materials are utilized, with the tensile stresses being primarily resisted by timber and the compression stresses by concrete. The degree of composite action between the two materials arises from the use of shear connectors, which provide resistance to interlayer slip. Ideally, the shear connectors should be sufficiently stiff under service loads to ensure a high degree of composite action, yet sufficiently soft to provide global ductility to the composite system at the ultimate limit state. As such, TCC systems are preferably designed to remain linear–elastic under the serviceability limit state, and to undergo nonlinear plastic deformation at the ultimate limit state as the shear connectors start to yield.

Several analytical methods have been developed for the analysis of TCC structures, each method with its own underlying assumptions and limited scope of application. The gamma method, currently adopted by Eurocode 5 (CEN 2004), is suitable for linear–elastic analysis of TCC members and is widely used in design. A linear–elastic analysis, however, is not expected to provide an accurate estimation of the failure load for ductile systems exhibiting pronounced nonlinear response.

Nonlinear methods that account for yielding of the shear connector include methods developed by Van der Linden (1999), Frangi and Fontana (2003), and Zhang and Gauvreau (2015). Van der Linden (1999) proposed a model that accounts for both elastic and plastic deformations of shear connectors and it assumes linear–elastic behaviour for concrete and timber. The method, however, does not allow for progressive yielding of the connectors resulting in an underestimation of the post-yielding stiffness. Frangi and Fontana (2003) proposed an elasto-plastic model suited to the assessment of the ultimate bending capacity of a TCC member. This procedure was developed for cases when failure occurs upon yielding of the connectors. The shear connectors are treated as having rigid – perfectly plastic behaviour. As such, this method cannot provide accurate estimations of stresses and deformations at serviceability limit state, unless highly stiff connectors are used. Zhang and Gauvreau (2015) proposed an analytical solution

Received 1 May 2020. Accepted 28 January 2021.

C. Liu. Morrison Hershfield Ltd., 125 Commerce Valley Dr. W #300, Thornhill, ON L3T 7W4, Canada.
A.C. Ferche. Department of Civil, Architectural and Environmental Engineering, The University of Texas at Austin, 301 E. Dean Keeton St. Stop C1700, Austin, TX, USA.
F.J. Vecchio. Department of Civil and Mineral Engineering, University of Toronto, 35 St. George St., Toronto, ON M5S 1A4, Canada.
Corresponding author: Anca-Cristina Ferche (email: ferche@austin.utexas.edu).

that combines the strengths of the gamma method and the Van der Linden model, producing a more accurate post-yielding load–deflection response over its predecessors. In this method, shear connectors are assumed to have linear – perfectly plastic behaviour and are allowed to yield progressively, while concrete and timber are considered to remain linear–elastic.

Concurrently with the development of analytical methods suited to the analysis of TCC elements, research efforts have been directed towards their implementation within nonlinear finite element analysis (NLFEA) software to enable both short-term and long-term loading analyses. Typically, concrete slab and timber beam systems were modelled with beam or shell elements, and the shear connectors were represented by discrete one-dimensional springs.

The model developed by Van der Linden (1999) was implemented within the finite-element program DIANA and it was used to analyze the response of TCC beams. The finite element (FE) model consisted of shell elements to represent the concrete slab, frame elements for the timber joist, and one-dimensional spring elements for the shear connectors. The FE model was used in conjunction with a Monte Carlo simulation to obtain a mean load–deflection response.

Fragiacomo and Ceccotti (2006) investigated the numerical modelling of TCC beams subjected to long-term loading. The approach assumed that shear strains were negligible and that plane sections remained plane. The FE model represented the concrete slab and the timber joist with two parallel beam elements connected with smeared one-dimensional spring elements that represented the shear connectors.

Persaud and Symons (2006) used the program Abaqus to model TCC specimens. Timber and concrete were modelled as linear–elastic materials represented by beam elements and the shear connectors were modelled as discrete spring elements with an empirically derived nonlinear force–displacement relationship. The numerical results were in good agreement with the experimental data up to approximately 50% of the failure load. However, the FE model underpredicted the deflection in the final load stages, potentially due to the material modelling of the concrete slab.

A comprehensive report by Dias et al. (2018) on the state-of-the-art of TCC recognized the current gap between research and design practice with respect to the use of FE analysis. The work presented in this paper aims, in part, to expand the range of application of FE analysis of TCC systems.

Toward the further development of NLFEA in this field, a two-dimensional FE model is proposed herein that considers material nonlinearity and yielding of shear connectors. The model was implemented within the algorithms of VecTor2, a two-dimensional nonlinear FE program developed at the University of Toronto, which has proven to be a reliable tool for the analysis of reinforced concrete structures (Ferche et al. 2017; Suseyto et al. 2013; Sagbas et al. 2011; Saatci and Vecchio 2009; Kim and Vecchio 2008; Palermo and Vecchio 2004). The somewhat rudimentary constitutive model implemented for timber performed well for the types of TCC specimens examined. For more challenging conditions, a more comprehensive constitutive model for timber may be required. The structure of the NLFEA program is such that a more encompassing model can easily be implemented as the need arises.

The primary value of the analysis procedure proposed herein is to provide accurate assessment capabilities at ultimate limit states. The verification studies undertaken show that the model performs well when calculating the behaviour of TCC specimens.

Mechanical behaviour of wood

Wood is an orthotropic material with three axes of symmetry: longitudinal, radial, and tangential. The longitudinal axis is parallel to the fiber, the radial axis is perpendicular to the growth rings, and the tangential axis is tangent to the growth rings. The mechanical properties along these axes are unique and independent.

Fig. 1. Typical stress–strain curves for wood (Republished with permission of Elsevier, from Holmberg et al. 1999; permission conveyed through Copyright Clearance Center, Inc.). [Colour online.]

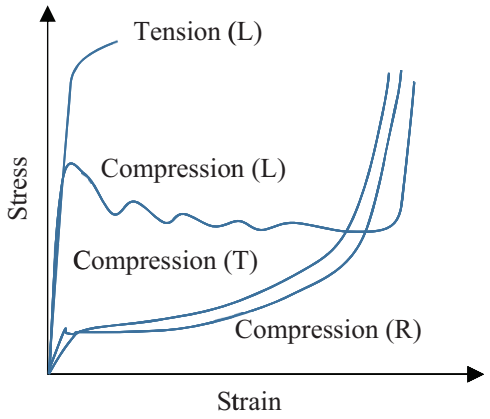

In the elastic region, wood obeys Hooke's generalized law for orthotropic materials. Therefore, the elastic properties can be described by 12 elastic constants, including three elastic moduli, three shear moduli, and six Poisson's ratios. The mechanical properties of wood differ with respect to species, moisture content, temperature, and density; however, relationships have been developed to relate one to another reasonably well (Bodig and Jayne 1982; Forest Products Laboratory 2010). Bodig and Jayne (1982) proposed the following relationships:

$$(1) \quad E_L : E_R : E_T \approx 20 : 1.6 : 1$$

$$(2) \quad G_{LR} : G_{LT} : G_{RT} \approx 10 : 9.4 : 1$$

$$(3) \quad E_L : G_{LR} \approx 14 : 1$$

Shown in Fig. 1 are typical stress–strain curves for wood loaded in tension in the longitudinal direction and in compression in the longitudinal, tangential, and radial directions (Holmberg et al. 1999). When subjected to axial tension along the longitudinal direction, wood behaves in a linear–elastic manner up to the proportional limit, followed by a reduced amount of plastic deformation. Such plasticity is often ignored by researchers in the field. By contrast, significant plasticity develops when wood is subjected to axial compression in the longitudinal direction. Compression in the radial and tangential directions yield similar stress–strain behaviour. For this reason, wood is sometimes regarded as a transversely isotropic material. Models describing the uniaxial behaviour of wood range from linear–elastic – perfectly plastic (Neely 1899) to linear–elastic followed by a linear descending branch (Bazan 1980), to a nonlinear seventh-order polynomial model (Glos 1978).

The failure modes of wood can be highly complex as they can be induced by one or more mechanical stimuli. Failure of a timber beam, for instance, may be caused by rupture of the tension fibers, delamination of fibers due to horizontal shear, buckling of the compression fibers, or a mix of all three. Several failure criteria applicable to wood, or to orthotropic composite material in general, are available in the literature (Hankinson 1921; Hill 1948; Azzi and Tsai 1965; Norris 1950; Hoffman 1967; Hashin 1980).

Structural behaviour of TCC components

TCC sections have been shown to be structurally efficient, with increased vibrational damping, increased in-plane rigidity, and superior sound insulation compared to an all-timber section (Dias et al. 2018). Their structural behaviour, however, is somewhat more complex than that of regular sections, in part because the mechanical

characteristics of wood and TCC are significantly different, and because the mechanical characteristics of the shear connectors dictate the stress distribution within the composite element. The degree of composite action depends heavily on the interlayer stiffness. There are three possible scenarios: full composite action, partial composite action, and no composite action. In the case of full composite action, the interlayer is considered to be infinitely rigid and therefore slip between timber and concrete layers cannot occur, whereas in the case of no composite action, the interlayer stiffness is assumed to be zero, allowing slip to occur freely. The actual degree of composite action of TCC systems generally lies between these two extremes.

A wide range of connection systems has been developed over the past decades, from simple nails to concrete notches reinforced with steel bars (Dias et al. 2018). These connection systems have unique load–slip responses determined through push-out or direct shear tests. In general, connection systems are evaluated in three aspects, including stiffness, strength, and ductility. Ideally, connection systems should be strong enough to resist the horizontal shear force along the interface, sufficiently stiff prior to yielding to ensure a high degree of composite action, and sufficiently ductile after yielding to provide overall ductility to the global TCC system.

For any TCC system to be efficient, three design criteria must be satisfied: the timber member must be strong enough to resist both bending and tension induced by gravity loads applied on the beam, the connection system must be sufficiently strong to transfer the design shear force and be sufficiently stiff to provide a high degree of composite action, and the connection system must be sufficiently ductile to provide overall ductility to the entire composite system.

The typical load–deflection curve for a TCC beam subjected to short-term bending starts with a linear–elastic branch followed by a nonlinear softening portion. Such nonlinearity is likely caused by cracking of concrete, buckling of wood fibers under compression, or progressive yielding of shear connectors (Persaud and Symons 2006; Deam 2008; Yeoh 2010; Gerber 2016). The failure of TCC beams generally arises from the rupture of wood fibers in the tension zone, particularly near knots or finger joints.

Overview of NLFEA procedure

The FE model for TCC structures proposed herein was implemented into the nonlinear FE program VecTor2 (VTAG 2019; Wong et al. 2013). The program employs a smeared rotating crack model for concrete and the solution procedure utilizes an incremental total-load, iterative secant, stiffness formulation. The disturbed stress field model (DSFM) (Vecchio 2000) forms the theoretical basis of the program. The DSFM is a smeared crack model, and is a hybrid formulation between a fully rotating crack model and a fixed crack model. Based on the modified compression field theory (Vecchio and Collins 1986), the DSFM considers equilibrium, compatibility, and constitutive relationships in terms of average stresses and strains measured over a gauge length greater than the crack spacing.

In VecTor2, wood is represented as a fixed orthotropic material with two axes of symmetry: parallel to the grain and perpendicular to the grain. This represents a significant deviation to how cracked concrete is modelled in VecTor2, where the axes of orthotropy typically rotate. Poisson's effect may not be neglected and the material stiffness matrix for wood, $[D_w]$, subjected to plane stress condition, is taken as

$$[D_w]' = \begin{bmatrix} \frac{1}{\overline{E}_L} & -\frac{\upsilon_{TL}}{\overline{E}_T} & 0 \\ -\frac{\upsilon_{LT}}{\overline{E}_L} & \frac{1}{\overline{E}_T} & 0 \\ 0 & 0 & \frac{1}{\overline{G}_{LT}} \end{bmatrix}^{-1} \quad (4)$$

Fig. 2. Analytical stress–strain curve for wood: (*a*) grain direction, and (*b*) transverse direction. [Colour online.]

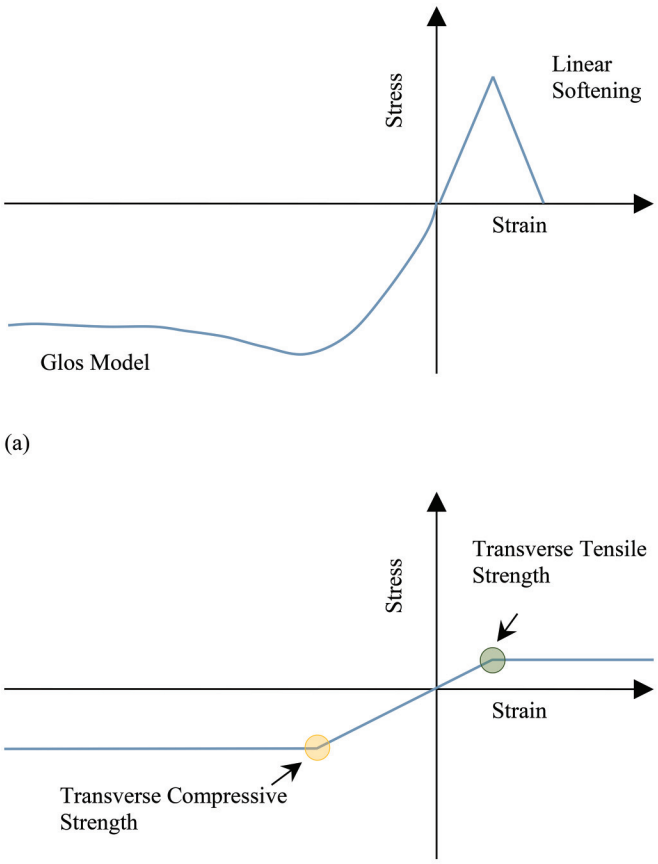

The secant moduli $\overline{E}_L, \overline{E}_L$, and $\overline{G}_L$ can be computed in a similar fashion as was done for concrete using the DSFM approach.

The accuracy of the constitutive model is critical as it heavily influences the material stiffness matrix. The constitutive model adopted in VecTor2 for wood consists of both linear and nonlinear branches. The Glos (1978) model is utilized for wood in compression, while linear–elastic behaviour is assumed for wood in tension up to peak tensile stress, followed by a linear softening branch. The linear softening branch is intentionally included for the modelling of timber structures reinforced with fiber-reinforced polymers. A typical stress–strain curve for wood in the grain orientation is shown in Fig. 2*a*.

The formulation of the Glos model is given as

$$\sigma = \frac{(\varepsilon/\varepsilon_1) + G_1(\varepsilon/\varepsilon_1)^7}{G_2 + G_3(\varepsilon/\varepsilon_1) + G_4(\varepsilon/\varepsilon_1)^7} \quad (5)$$

$$G_1 = \frac{100 f_s}{6E[1 - (f_s/f_c)]} \quad (6)$$

$$G_2 = \frac{1}{E} \quad (7)$$

$$G_3 = \frac{1}{f_c} - \frac{7}{6E} \quad (8)$$

$$G_4 = \frac{G_1}{f_s} \quad (9)$$

where σ is the stress, ε is the net strain, ε_1 is the strain corresponding to maximum stress, f_s is the residual stress, E is Young's modulus, and f_c is the maximum compression stress.

The Glos model can be simplified using the following relations:

$$f_s = 0.8 f_c \quad (10)$$

$$\varepsilon_1 = 0.008 \sim 0.012 (0.010) \quad (11)$$

$$\varepsilon_u \approx 3\varepsilon_1 \quad (12)$$

The stress–strain behaviour in the transverse direction is approximated as linear–elastic–plastic for both compression and tension. The elastic modulus is taken as 5% of that in the longitudinal direction. A typical stress–strain curve for wood in the transverse orientation is presented in Fig. 2*b*.

The shear connectors connecting the timber and the concrete components can be modelled by bond–slip elements. VecTor2 has two built-in bond–slip elements: link elements and contact elements. The link element is a non-dimensional element defined by two different nodes sharing the same coordinates prior to slippage. It may be idealized as two springs orthogonal to one another. One spring deforms tangentially to the connected elements while the other spring deforms perpendicular to the connected elements. The contact element is a four-noded element with the four nodes defining the element divided into two-node pairs. Like the link element, the nodes within each node pair share identical coordinates prior to slippage. The contact element represents a continuous interface along the shared edge of the connected elements. The displacement of any point along the contact element is linearly interpolated from the nodal displacements to ensure compatibility of the connected elements.

Because the link element is dimensionless, it is suitable for situations where the shear connectors are concentrated at distinct locations, such as with screw- or dowel-type fasteners. By contrast, the contact element may be considered as a more flexible and realistic representation of shear connectors. The contact element may be used to model concentrated connectors, as well as those connectors that are large in size such as notched concrete connections, or those that are continuous along the span, such as continuous metal plate connections.

In VecTor2, the load–slip behaviour of the connectors is approximated by a piecewise linear curve. An example of this approximation is shown in Fig. 3, in which the real load–slip behaviour of screw connectors tested by Persaud and Symons (2006) was approximated by three line segments. The piecewise curve is defined by four reference points connected with straight lines. By default, the origin is used as one of the reference points and the remaining three points are manually input by users. It should be noted that the load–slip relation must be first converted to the stress–slip domain simply by dividing the resistance force by the tributary area of the contact element.

Because wood is modelled as a fixed-orthotropic material subjected to biaxial stress, three alternative failure criteria may be applicable to the scenario: the Azzi and Tsai (1965) criterion, the Norris (1950) criterion, and the Hashin (1980) criterion. The Hashin criterion has been implemented in VecTor2 to account for the different types of failure modes, and characterizes wood failure by four scenarios: fibre tension

$$\frac{\sigma_L^2}{f_{L,t}^2} + \frac{\tau_{LT}^2}{f_{L,v}^2} = 1 \quad (13)$$

Fig. 3. Multilinear approximation (adapted from Persaud and Symons 2006). [Colour online.]

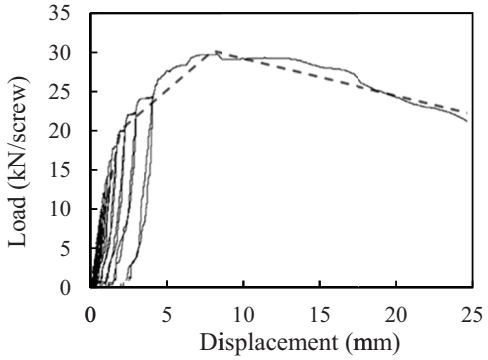

fibre compression

$$\frac{\sigma_L}{f_{L,c}} = 1 \quad (14)$$

matrix tension

$$\frac{\sigma_T^2}{f_{T,t}^2} + \frac{\tau_{LT}^2}{f_{L,v}^2} = 1 \quad (15)$$

and matrix compression

$$\frac{\sigma_T^2}{4f_{T,v}^2} + \left[\left(\frac{f_{T,c}}{2f_{T,v}}\right)^2 - 1\right]\frac{\sigma_T^2}{f_{T,c}^2} + \frac{\tau_{LT}^2}{f_{L,v}^2} = 1 \quad (16)$$

where $f_{L,t}$, $f_{L,c}$, $f_{T,t}$, $f_{T,c}$, $f_{L,v}$, and $f_{T,v}$ are the strengths related to longitudinal tension and longitudinal compression, transverse tension and transverse compression, and longitudinal shear and transverse shear, respectively.

For flexure-critical timber beams, failures typically occur at the bottom of the beam, where the wood fiber is essentially subjected to uniaxial tensile stress. In this scenario, both eqs. (15) and (16) will be equal to zero on the left-hand side, and the matrix failure mode will never govern the ultimate failure. Moreover, the second term of eq. (13) is zero, and therefore the Hashin criterion is reduced to the uniaxial failure criterion, which is the same as the Rankine criterion.

For shear-critical conditions, failures are more likely governed by a combination of shear stress and axial stress, and the matrix failure modes become more prominent. However, it should also be pointed out that the transverse tensile strength and the transverse shear strength are the less commonly known mechanical properties of wood; their values are typically not available in the literature.

Modelling of timber specimens

The experiment series conducted by Gentile (2000), chosen as the verification study, consisted of 22 half-scale timber beams and four full-scale timber beams tested to failure. This analytical study was performed to evaluate the accuracy of the proposed methodology in simulating the response of timber specimens prior to modelling TCC beams. All specimens were simply supported and tested under four-point bending. Among the specimens, 15 of the half-scale specimens and three of the full-scale specimens were reinforced with glass fiber-reinforced polymer (GFRP) bars, with the remaining plain timber beams serving as control specimens. Epoxy resin was used to bond the GFRP bars to the timber, creating a perfect bond condition.

For all the half-scale specimens, the cross section was 100 mm × 300 mm, with a load span of 600 mm, and a support span of

Fig. 4. FE mesh for half-scale timber beams with GFRP reinforcement. [Colour online.]

4000 mm. The GFRP bars were installed in the grooves that were cut 30 mm above the bottom fibers into the sides of the specimens. The grooves had a constant depth of 25 mm, and varying width to accommodate different numbers of GFRP bars. For the four full-scale specimens, the cross section was 200 mm × 600 mm with a load span of 1200 mm and a support span of 10.0 m. Due to the available lengths of the GFRP bars used, only the central 6.0 m was reinforced.

Both the plain timber specimens and the reinforced timber specimens were modelled in VecTor2 using the auto-meshing function, with only half of the span modelled due to symmetry. Rectangular membrane elements were used to model the timber, while truss elements were used to model the GFRP bars. Perfect bonding was assumed between the GFRP bars and the timber. A typical FE model is shown in Fig. 4.

The modulus of elasticity and the modulus of rupture in the longitudinal direction were reported by Gentile (2000); these values were used as the input mechanical properties of timber. The modulus of rupture, a flexural failure test, may be used as the tensile strength parallel to the grain, although it is not a true stress because the formula by which it is calculated is valid only within the elastic range.

For a FE analysis, apart from the modulus of elasticity and the modulus of rupture, other material inputs are required, namely, the tensile strength perpendicular to the grain, the compressive strength parallel to the grain, the compressive strength perpendicular to the grain, and the shear strength. Representative values may be found in the Wood Handbook (Forest Products Laboratory 2010). However, these values were obtained from small defect-free samples, which may not be appropriate for full-scale structural grade timber. Therefore, reasonable assumptions were made as follows:

1. The magnitude of the longitudinal compressive strength was taken as equal to that of the longitudinal tensile strength.
2. The tensile strength perpendicular to the grain and the shear strength were assumed to be 10% of the tensile strength parallel to the grain, while the transverse compressive strength was assumed to be 20% of that of the longitudinal counterpart.
3. Lastly, the elastic modulus perpendicular to the grain orientation was calculated based on relationships proposed by Bodig and Jayne (1982). Additional details are given in Liu (2016).

Given in Fig. 5 are typical load–deflection plots, showing comparisons between the VecTor2 simulation results and the experimental results, presented as the red dotted line and black solid line, respectively. In general, the NLFEA model was capable of predicting the pre-peak global load–deflection responses and the global stiffness with sufficient accuracy. Table 1 presents the ultimate loads calculated by VecTor2, which agreed well with the experimental measurements. The only exception was specimen D2, in which the failure occurred outside of the constant moment region, causing an underestimation of the modulus of elasticity.

The post-peak ductility for the reinforced specimens was also reasonably well captured. For additional information on modelling the Gentile (2000) specimens, the reader is referred to Liu

Fig. 5. Typical load–deflection plots for timber specimens: (*a*) half-scale specimen D1, and (*b*) full-scale specimen FS-1. [Colour online.]

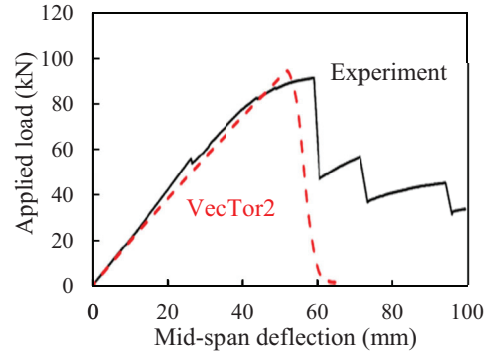

(a)

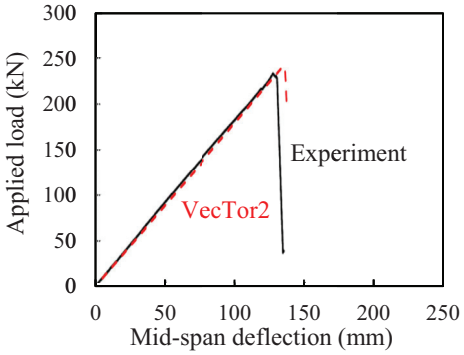

(b)

(2016). In general, the reinforced specimens exhibited more post-peak ductility than those without reinforcement. Specimen F2, with a modulus of elasticity of 6039 MPa and a modulus of rupture of 23 MPa, exhibited a smooth and ductile post-peak response with only 0.27% reinforcement. To the contrary, specimen D1, while having the same amount of reinforcement and being approximately two times stronger and stiffer than specimen F2, experienced a brittle failure as the applied load and the stiffness dropped rapidly once the maximum force was reached. Specimen I2 had a reinforcement ratio of 0.82%, and demonstrated a more ductile post-peak response than that of specimen D1. Based on the preceding observations, it may be concluded that the amount of post-peak ductility depended not only on the reinforcement ratio, but also the quality of the timber.

Regarding the failure modes, tension failure was predicted by the NLFEA model in the constant moment region for all specimens; whereas, as per Gentile (2000), the failure modes of the specimens included tension failure, compression failure, and flexural-shear failure, which was only found in three of the reinforced specimens. Because of the lack of information, the specimens that had flexural-shear failures were excluded from the analysis. All plain timber beams failed in brittle tension with no signs of crushing in the compression zone, which was in agreement with the analysis predictions. While all the reinforced specimens initially developed tensile cracks in the constant moment region, half of them experienced ductile compression failure due to crushing of wood fiber in the top face. Unfortunately, Gentile (2000) did not identify the failure modes of individual specimens and therefore it was impossible to proceed any further with the analysis of failure modes. Nevertheless, it was believed that the analysis model was unable to predict the ductile compression failures for two possible reasons as follows: the true compressive strength

Table 1. Summary of results for the Gentile (2000) specimens.

Beam ID	P_u (kN) Exp.	P_u (kN) VecTor2	P_u(VecTor2)/P_u(exp.)
A1	36.9	34.6	0.94
A2	75.8	82.0	1.08
B1	37.5	35.8	0.95
C1	64.7	63.0	0.97
D1	92.6	95.2	1.03
D2	85.7	60.0	0.70
F1	32.5	31.0	0.95
F2	40.0	40.0	1.00
G1	76.5	72.2	0.94
G2	77.4	85.4	1.10
H1	43.5	41.6	0.96
H2	55.9	58.4	1.04
I1	107.5	111.0	1.03
I2	103.0	90.0	0.87
J1	34.4	32.6	0.95
K1	65.1	68.2	1.05
L1	47.2	50.6	1.07
L2	59.6	69.0	1.16
FS-1	236.0	243.0	1.03
FS-2	296.0	298.6	1.01
FS-3	191.0	212.4	1.11
FS-4	132.0	126.4	0.96
		Mean	1.00
		SD	0.10
		COV	9.57%

of timber was not reported in the original literature and was assumed to have the same magnitude as the tensile strength, and the presence of GFRP bars hindered the propagation of tension-initiated cracks, leading to a much more ductile post-cracking tensile response of the timber. Although the currently adopted constitutive model included a simple linear softening branch in tension, its appropriateness was not validated experimentally.

The perfect-bonding assumption of the numerical models agreed well with the experimental observations. Although localized debonding of GFRP bars adjacent to tensile cracks was present, none of the failures were caused by debonding or delamination of the reinforcement.

Based on this verification study, it was concluded that the simple constitutive models adopted, and the assumptions made for the unknown mechanical properties of wood, were appropriate in general for flexure-critical conditions. Because of the lack of information on specimen material properties, the NLFEA model as implemented in VecTor2 was unable to capture the compression failures observed in some of the reinforced specimens. Nevertheless, it was able to predict the global stiffness, the failure loads, and the initial cracks initiated by tension with sufficient accuracy.

Modelling of TCC beams

Following the successful analytical results for plain timber specimens, numerical modelling of TCC beams subjected to short-term monotonic loadings was investigated. Despite the fact that the experiments performed by different researchers varied considerably in terms of dimensions, load configurations, mechanical properties, materials, and the types of shear connector, all the FE models created in the verification studies undertaken share the following similarities:

1. All models consist of two basic elements: membrane elements and contact elements. The membrane elements were used to model the timber and the concrete components, while the contact elements were used to represent the shear connectors.
2. Bearing plates were introduced to all the models to mitigate high local stress for the elements directly in contact with the supports and the loading jacks. The bearing plates were also modelled with membrane elements.
3. A number of the specimens had interlayers (e.g., particle board) between the concrete and the timber members. Such interlayers were treated as an integral part of the underlying timber members, and were assumed to have the same mechanical properties. It is possible that this simplification could result in an overestimation of the global stiffness as the interlayers are likely softer than the timber member. Moreover, the presence of interlayer reduces the penetration depth of the shear connectors into the timber members, which can cause a reduction in the stiffness and load-carrying capacity of the shear connectors.

A sample FE model with an exaggerated depth-to-span ratio is presented in Fig. 6*a*. This general model represents a TCC beam subjected to four-point bending. Due to symmetry, only half of the beam is modelled. For the purpose of illustration, the model has a coarse mesh and includes all the possible components as discussed, with the concrete, the timber, and the interlayer components shaded in grey, brown, and yellow, respectively. The blue and green elements represent the loading plate and bearing pad, respectively. The red line between the concrete and the interlayer depicts the smeared contact elements, representing continuous shear connectors. Alternatively, the shear connectors may be modelled as discrete, as shown in Fig. 6*b*.

While VecTor2 has a number of built-in advanced material and behavioural models implemented for concrete, only simple (default) models were used for the verification studies. Additional details on the modelling aspect can be found in Liu (2016). As per the published literature (Persaud and Symons 2006; Ceccotti et al. 2007), the global failure of TCC beams is rarely governed by the concrete component; therefore, there was no need to use the advanced models that were implemented for specific case scenarios. For concrete, a minimum of one input parameter is required to characterize the material: the cylinder compressive strength. Unless otherwise specified, the other mechanical properties are calculated using the default relationships (Wong et al. 2013).

Owing to the orthotropic nature of wood, the required input parameters for timber are quite extensive. The majority of these required inputs were not available from the original literature, including the longitudinal compressive strength, the transverse compressive and tensile strength, and the shear strength, as well as Poisson's ratios. As mentioned previously, the appropriateness of the mechanical properties suggested in the Wood Handbook (Forest Products Laboratory 2010) to represent full-scale structural timber is questionable. The longitudinal tensile strength of the specimens, on the other hand, was reported in most studies. The source of these values was typically from the manufacturers' specifications or, occasionally, from design guidelines, such as the Eurocode 5. These values are inherently conservative as they are intended for practical use by design engineers; use of these values in the FE models likely results in an early termination of the analysis once the longitudinal tensile strength of wood is reached.

Based on the aforementioned circumstances and the limited availability of data, a number of assumptions and simplifications were adopted to make the subsequent validations possible, including the following:

1. The published longitudinal tensile strength was used as a starting point for all the FE models; however, in case of early

Fig. 6. Timber-concrete FE models: (*a*) sample FE model with smeared connectors, and (*b*) sample FE model with discrete shear connectors. [Colour online.]

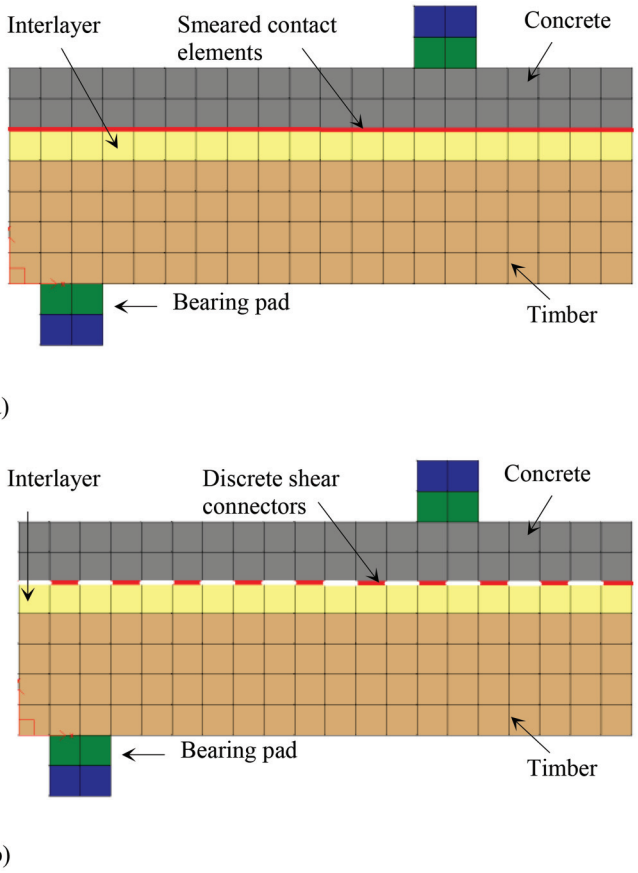

Fig. 7. Experimental versus calculated response for Persaud and Symons (2006) TCC slab (adapted from Persaud and Symons 2006): (*a*) load–deflection behaviour, and (*b*) load–slip response. [Colour online.]

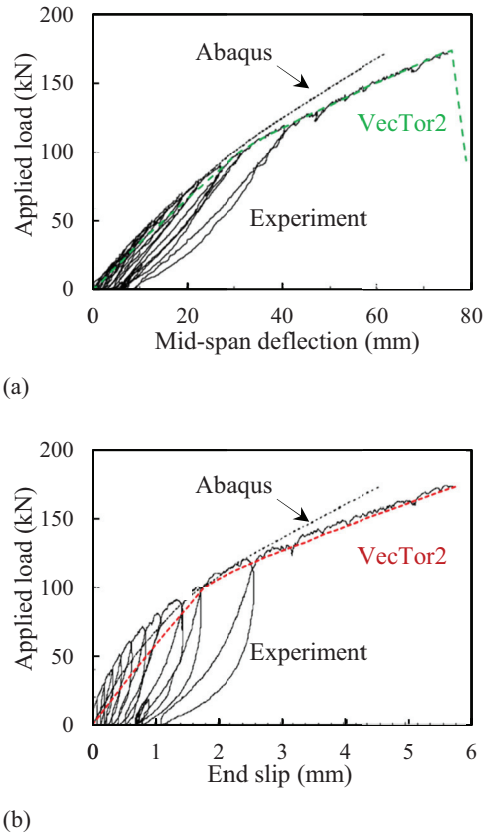

termination of the analysis, the longitudinal tensile strength was progressively increased to ensure that a complete global load–deflection response was replicated.

2. The predominant failure mode of plain timber beams is through tensile failure of the bottom fiber, typically initiated near knots or finger-joints. The implication of this experimental observation is that the longitudinal compressive strength is likely as strong as the longitudinal tensile strength, if not stronger. Therefore, unless explicitly stated in the literature, the magnitude of the longitudinal compressive strength was taken as equal to that of the longitudinal tensile strength.
3. The transverse tensile strength was assumed to be 10% of the longitudinal tensile strength while the transverse compressive strength was taken as 20% of the longitudinal compressive strength. These assumptions are largely consistent with the values published in the Wood Handbook (Forest Products Laboratory 2010).
4. Although the Wood Handbook (Forest Products Laboratory 2010) suggests that the shear strength parallel to the grain may be taken as 20%–25% of the longitudinal compressive strength, 10% was adopted in the FE models to account for the fact that the timber types used in the experiments were engineered wood products, such as laminated-veneer lumber, glued-laminated timber, and cross-laminated timber (CLT). These engineered wood products contain not only natural defects, but also artificial defects, such as finger-joints or inadequate glue between the layers. In fact, rolling shear failure is a common type of failure found in CLT.
5. As density and Poisson's ratios have a small influence on the numerical results, these values were taken directly from the Wood Handbook (Forest Products Laboratory 2010).
6. The transverse Young's modulus was taken as 5% of the longitudinal Young's modulus as per the relations proposed by Bodig and Jayne (1982).

The load–slip relationship of the shear connectors is specified as an input in VecTor2. The load–slip relationship is approximated by a piecewise curve, as discussed previously, and must be converted to stress–slip format by converting the force to an equivalent stress.

A full-scale TCC floor slab was constructed and tested under three-point bending to failure at the University of Cambridge (Persaud and Symons 2006). The proposed system used ordinary zinc-plated steel coach screws as the shear connectors and a thin ribbed steel decking system to act as a permanent formwork for the cast-in-place concrete floor slab. Smeared contact elements were used in the FE models, with the analytical load–slip curve adapted from the experimental results obtained by Persaud and Symons (2006), presented in Fig. 3.

Figure 7*a* shows the experimental load–deflection response versus the predicted load–deflection response, while Fig. 7*b* compares the predicted and the experimental load–slip curves measured at the beam end. The dotted lines included in both plots are the analytical results obtained from a 2D Abaqus model created by Persaud and Symons (2006). Overall, the complete load–deflection response was captured well by VecTor2, better than was done with Abaqus. A mid-span deflection of 75.6 mm and a failure load of

Fig. 8. Deflected shape for Persaud and Symons (2006) TCC slab at collapse (5× magnification). [Colour online.]

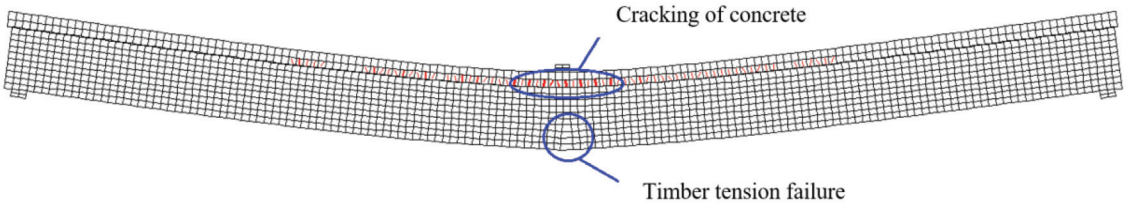

173.6 kN were predicted by VecTor2 while the actual mid-span deflection and failure load were 74.9 mm and 173 kN, respectively. Moreover, VecTor2 predicted tension failure at mid-span, which was consistent with the experimental observation that the final collapse of the specimen was initiated in the region of a knot in the bottom laminates. An exaggerated deflected shape (5× magnification) of the TCC specimen is depicted in Fig. 8. One major discrepancy between the experimental result and the NLFEA prediction was that the latter indicated concrete cracking near the mid-span directly under the loading jack, whereas in the experiment, no cracking was observed. Such a discrepancy may be attributed to the confining effect of the steel decking, which may have prevented the concrete slab from cracking.

Eleven full-scale TCC beams were tested in four-point bending at the University of Canterbury in New Zealand by Yeoh (2010). Four connection types were used in these specimens, including metal plates pressed onto the timber beams, triangular notches, and small and large rectangular notches cut from the timber beams.

A summary of the numerical results is presented in Table 2. In general, the experimental load–deflection curves and the failure loads were reasonably well predicted by the analyses. Note that specimen D1 was not loaded to complete destruction. Specimens B1, C1, C2, E1, and F1 experienced brittle tension failure while progressive tension failure was found in specimen G1. The failure modes of the rest of the specimens were not reported in the literature. Some degree of post-peak strength recovery observed in specimens B2 and F1 was not properly captured in the analyses. Also, the stiffnesses of specimens B1, B2, E1, and E2 were somewhat underestimated. As a natural material, wood properties vary considerably. Consequently, the source of error could be solely from the natural variability of the modulus of elasticity of wood, which was assumed to be identical across all specimens.

Notably, the predicted stiffness of specimen F1 deviated from the experimental result at large loads. In this case, the spacing effect of the shear connectors could be ultimately responsible for the deviation. The shear connectors were closely spaced near the support. Ceccotti et al. (2007) tested two push-out test specimens with variable spacing and found a clear distinction between the corresponding load–slip curves. Specimen G1, contrary to the brittle tension failure predicted by the analysis, exhibited substantial post-peak ductility. No signs of connector failure were observed experimentally, and the unusual plateau resulted from the progressive tension failure in the timber beam. The currently adopted timber constitutive model is inadequate for replicating such types of failure.

Another series of specimens tested at the University of Canterbury by Deam et al. (2008) was selected for the verification studies. Two of the specimens, CS3 and CS4, were prestressed with low relaxation 7-wire stranded tendons and different connection systems were investigated: 24 notches with screws for specimen CS1, end-bearing bolted saddles for specimen CS2, 48 notches with screws for specimen CS3, and 24 lag screws for specimen CS4.

No analysis was performed for specimen CS2 since there was no push-out test performed for the novel connection system. While it is theoretically possible to model the draped tendon profile in specimen CS4, it is currently impractical to do so because the current version of auto-meshing functionality of VecTor2 is not applicable to TCC structures. To capture the draped tendon profile, a series of nodes must be created in line with the tendon profile and the bounded elements must be either triangular or quadrilateral. As such, specimen CS4 was also excluded from the analysis. The load–deflection response was captured with sufficient accuracy for specimen CS1 and the results are summarized in Table 2.

Eighteen TCC panels were tested at the University of British Columbia by Gerber (2016). These panels, unlike typical TCC beams, had uniform thickness over their depth. Nevertheless, the observed load–deflection behaviour of this series agreed fairly well with that of the TCC beams investigated previously. All the specimens were modelled with the same approach described in the previous three experiment series. Four panels were constructed with CLT. Typically, CLT consists of an odd number of layers of timber boards stacked together in alternating directions; the direction with one extra layer of timber board is hereinafter referred to as the primary direction, whereas the orthogonal direction is denoted as the secondary direction. The intent of CLT is to have an improved stiffness in the secondary direction at the cost of a reduced stiffness in the primary direction. Consequently, it may be inappropriate to model CLT as a whole; the alternating layers must be reflected in the corresponding FE model.

While the initial stiffness of the CLT specimens was well captured in the analyses, the stiffness at large loads was overestimated by 9% on average. This may be attributed to the weaker sandwiched layer. According to the literature, it is common industry practice to use timber boards of lower grade as the inner layers of CLT. Rolling shear failure, a common type of failure found in CLT, may also contribute to the deviation in stiffness. As a result of the nonuniform distribution of glue strength, this type of failure typically occurs at locations where the shear stress demand exceeds the local glue strength. At the onset of rolling shear failure, the applied shear stress must be redistributed to the adjacent glue, causing a reduction in the global stiffness. Moreover, since the specimens were loaded under displacement control, the stress redistribution also gave rise to a series of sudden drops in force observed in the global load–deflection curves. The results are summarized in Table 2.

The precision of a FE analysis is normally heavily dependent on the mesh size. To obtain stable analysis result, the mesh size must be sufficiently fine. The mesh size of an FE model is considered to be adequate if further refinement of the mesh size yields no significant changes to the analysis results.

Figure 9 presents the FE models, both created for specimen CS1 tested by Deam et al. (2008). Identical input parameters were used in each model. The model with the finer mesh had a grid size of 25 mm × 25 mm, which was three times finer than that of the model with a coarse mesh. While the finer mesh is much more computationally demanding, the calculated load–deflection responses are practically identical, as depicted in Fig. 10. The model with a finer mesh did terminate earlier as a result of higher average stress

Table 2. Summary of results for the TCC specimens.

	Experiment		Analytical		Comparison	
Beam ID	P_u (kN)	Displ. (mm)	P_u (kN)	Displ. (mm)	P_u(VecTor2)/ P_u(exp.)	Displ.(VecTor2)/ Displ.(exp.)
Persaud and Symons 2006						
PS1	173	74.9	173.6	75.6	1.00	1.01
Yeoh 2010						
A1	87.5	63.9	89.6	77.5	1.02	1.21
A2	75.1	63.0	89.6	77.5	1.19	1.23
B1	104.9	63.0	99.8	67.7	0.95	1.07
B2	98.1	63.6	98.4	67.6	1.00	1.06
C1	89.1	58.2	101.8	65.4	1.14	1.12
C2	109.7	66.8	101.8	65.4	0.93	0.98
E1	79.4	92.2	80.4	96.2	1.01	1.04
E2	55.9	66.4	79.0	96.9	1.41	1.46
F1	175.0	89.8	176.4	76.8	1.01	0.86
G1	201.1	69.2	199.2	67.6	0.99	0.98
Deam 2008						
CS1	158.5	77.7	158.5	89.0	1.00	1.15
Gerber 2016						
VG3-1	128.6	161.6	134.2	160.4	1.04	0.99
VG3-2	114.4	148.5	134.2	160.4	1.17	1.08
VG6-1	125	182.8	137.2	150.9	1.10	0.83
VG6-2	124.5	174	137.2	150.9	1.10	0.87
VG10-1	73.8	117.6	104.6	125.37	1.42	1.07
VG10-2	92.6	117.4	104.6	125.37	1.13	1.07
VG15-1	120.5	125	103.6	92.5	0.86	0.74
VG15-2	102.7	116.3	103.6	92.5	1.01	0.80
AB6-1	104.5	112.2	100.2	88.7	0.96	0.79
AB6-2	86.4	254.1	100.2	88.7	1.16	0.35
GM1-1	88.7	120.5	97.6	129	1.10	1.07
GM1-2	86.7	127.5	97.6	129	1.13	1.01
GM2-1	87.8	115	94.2	101.3	1.07	0.88
GM2-2	89.5	102	94.2	101.3	1.05	0.99
GM4-1	84.4	119.2	81.4	91.2	0.96	0.77
GM4-2	74.11	102.9	81.4	91.2	1.10	0.89
GM6-1	90.4	80.1	97.6	73.2	1.08	0.91
GM6-2	90	75	97.6	73.2	1.08	0.98
				Mean	1.07	0.97
				SD	0.12	0.19
				COV	11%	19.60%

within the critical element. Nevertheless, the model with a coarse mesh can be considered as adequately meshed.

Since nonlinear material constitutive models were adopted in VecTor2, it is important to examine the contribution of the nonlinear models to the global nonlinearity of the composite system. To do this, the material responses were set to linear–elastic models such that the shear connectors were the only source of nonlinearity of the global system. Figure 11*a* compares the numerical results of specimen CS1 (Deam et al. 2008) with linear and nonlinear material models. While the linear material models yielded a slightly stiffer result, the difference was rather negligible. A similar comparison was performed for specimen S7 tested by Gerber (2016); the results are presented in Fig. 11*b*. This time, the linear material models yielded a noticeably stiffer load–deflection response than that of the nonlinear material models. The major distinction between the two specimens was the specimen configuration. The concrete slab of specimen S7 had a depth of 70 mm and a total depth of 159 mm, while specimen CS1 had the same depth of concrete slab but the total depth of the specimen was 448 mm.

Therefore, for a TCC beam of typical configuration where the depth of the concrete slab is relatively thin compared to the total depth of the specimen, the global load–deflection response is generally not sensitive to material nonlinearity. However, for a TCC beam with a higher percentage of concrete depth with respect to the total depth, inclusion of nonlinear material models may yield more accurate results.

Conclusion

The goal of this work was to investigate the potential capability of NLFEA procedures to accurately model the behaviour of TCC structures subjected to short-term loadings, and to gain some insight into the nature of the constitutive models best suited for this purpose. Appropriate constitutive models describing the nonlinear behaviour of wood were determined from the literature and implemented in NLFEA program VecTor2. Verification of the constitutive models and analysis procedure was then undertaken by modelling plain and reinforced timber beams subjected to short-term monotonic flexure. Finally, modelling of TCC beams subjected to short-term monotonic flexure was conducted for numerous specimens varying in size, test setup, specimen configuration, materials, and types of shear connectors.

From the results of the verification studies performed, the following conclusions were derived:

1. NLFEA procedures based on a total-load, secant-stiffness algorithm is a viable approach for modelling structural elements comprising plain timber or timber composite such as timber – fiber-reinforced polymer or TCCs.

Fig. 9. FE models with different mesh sizes: (*a*) coarse mesh, and (*b*) fine mesh. [Colour online.]

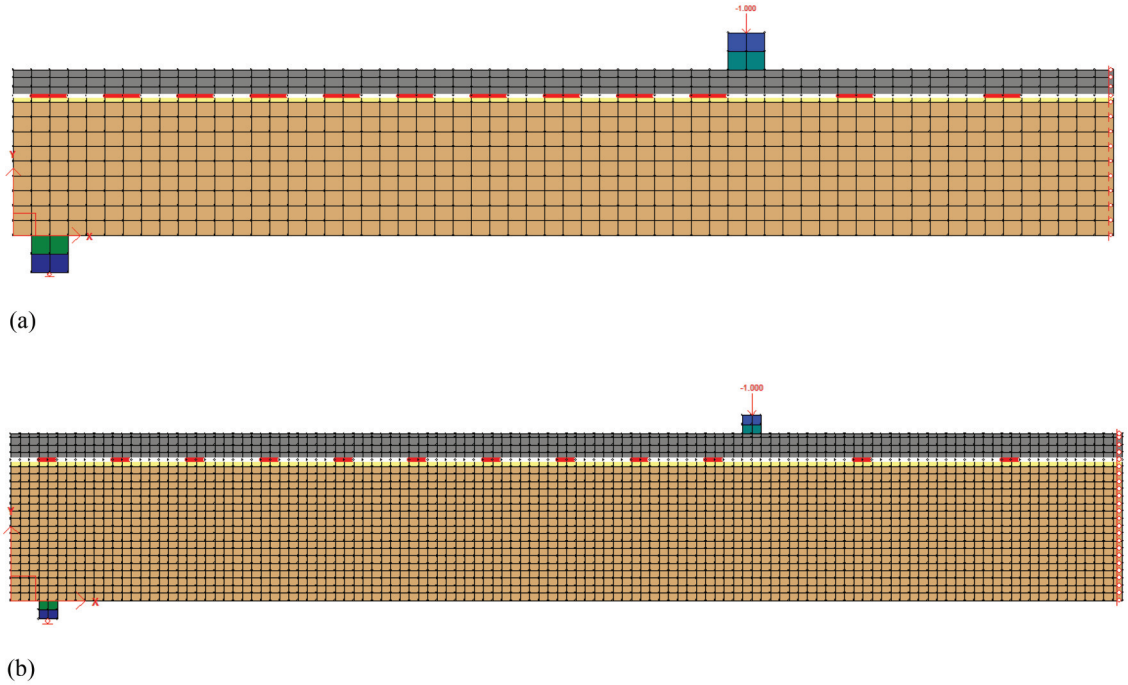

Fig. 10. Comparison of predicted load–deflection responses of different mesh sizes. [Colour online.]

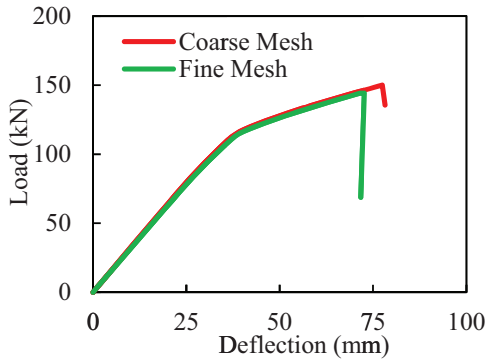

Fig. 11. Load–deflection responses: linear versus nonlinear concrete constitutive models: (*a*) specimen CS1, and (*b*) specimen S7. [Colour online.]

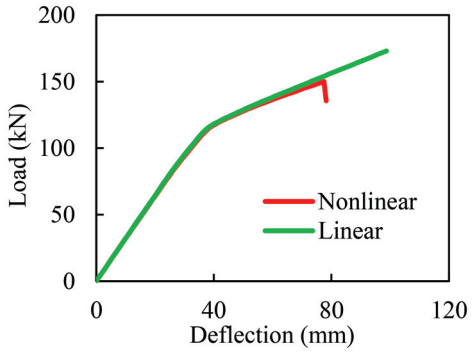

(a) Specimen CS1

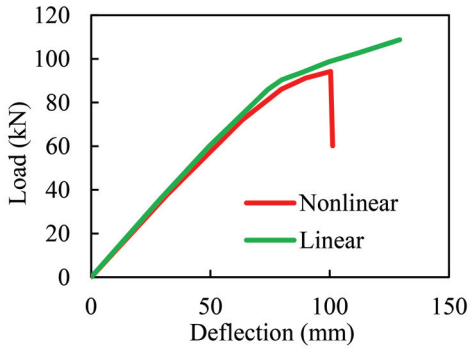

(b) Specimen S7

2. Wood can effectively be modelled as a fixed orthotropic material, while concrete can be treated as an orthotropic material based on the smeared rotating crack approach.
3. The Hashin failure criterion, coupled with appropriate assumptions found in the literature for the various strength and mechanical properties of wood, enables accurate predictions of strength, load–deflection response, ductility, and failure mode for timber and TCC systems.
4. The capabilities of NLFEA have been examined for flexure-critical TCC beams subjected to short-term monotonic loadings only. Capability to perform dynamic analysis of TCC structures is uncertain.
5. The true tensile strength, as determined from the failure loads of the beam specimens examined, is generally 30%–50% higher than the mean suggested by the manufacturers.
6. The performance of TCC is largely dictated by the load–slip relationship of shear connectors. As illustrated by Yeoh (2010), the degree of composite action can be close to 100% if the shear connectors are sufficiently stiff. It was also observed that the load–deflection remains fairly linear up to failure.

The implication of this observation is that a high degree of composite action is achieved at the cost of reduced global ductility.

7. Shear connectors may be modelled using smeared (contact) or discrete (link) elements, depending on the connection type and the layout of shear connectors. For shear connectors with constant spacing or shear connectors that are installed continuously along the span, such as metal plate connectors, the smeared contact elements may be a better option, whereas the discrete link element is more suitable for connectors without uniform spacing. The elastic–plastic behaviour found with most connectors should be represented in the modelling.
8. The size of the shear connectors in full-scale specimens should be consistent with that tested in the calibration push-out tests. As demonstrated in Deam et al. (2008), the accuracy of the analysis is compromised when the sizes of shear connectors do not match those of the full-scale bending specimens.
9. The spacing effect should be taken into consideration in the push-out tests. The load–slip relationship can vary considerably as a function of spacing.
10. Generally, the load–deflection response of a TCC member is well predicted if the ultimate failure is caused by either the timber beam rupturing due to high tensile stress in the wood fiber or by crushing of concrete; however, crushing of concrete is a less common type of failure for TCC specimens.
11. Although cracking of concrete was predicted for all the specimens investigated, it was not experimentally observed in the TCC specimens with an interlayer acting as a permanent formwork for the concrete slab. However, Van der Linden (1999) tested 20 TCC specimens without such interlayers and found visible cracks, which first occurred directly underneath the loading jacks. This suggests that the presence of an interlayer may confine or cushion the bottom concrete from cracking.

References

Azzi, V.D., and Tsai, S.W. 1965. Anisotropic strength of composites. Experimental Mechanics, **5**(9): 283–289. doi:10.1007/BF02326292.

Bazan, I.M.M. 1980. Ultimate bending strength of timber beams. Ph.D. dissertation, Nova Scotia Technical College, Halifax, NS.

Bodig, J., and Jayne, B.A. 1982. Mechanics of wood and wood composites. Van Nostran-Reinhold Co. Inc., New York, NY.

Ceccotti, A. 2002. Composite concrete-timber structures. Progress in Structural Engineering and Materials, **4**: 264–275. doi:10.1002/pse.126.

Ceccotti, A., Fragiacomo, M., and Giordano, S. 2007. Long-term and collapse tests on a timber-concrete composite beam with glued-in connection. Materials and Structures, **40**: 15–25. doi:10.1617/s11527-006-9094-z.

CEN. 2004. Design of timber structures – Bridges. Eurocode 2: Part 2. Comité Européen de Normalisation (CEN), Brussels, Belgium.

Deam, B., Fragiacomo, M., and Gross, L. 2008. Experimental behaviour of prestressed LVL-concrete composite beams. Journal of Structural Engineering, ASCE, **134**(5): 801–809. doi:10.1061/(ASCE)0733-9445(2008)134:5(801).

Dias, A., Schanzlin, J., and Dietsch, P. 2018. Design of timber-concrete composite structures. COST Action FP1402/WG 4, pp. 228.

Ferche, A.C., Panesar, D.K., Sheikh, S.A., and Vecchio, F.J. 2017. Toward macro-modeling of alkali-silica reaction-affected structures. Structural Journal, **114**(5): 1121–1129. doi:10.14359/51700778.

Forest Products Laboratory. 2010. Wood handbook: wood as an engineering material. General Technical Report FPL-GLR-190. U.S. Department of Agriculture, Forest Service, Forest Products Laboratory, Madison, Wisc.

Fragiacomo, M., and Ceccotti, A. 2006. Behavior of timber-concrete composite beams. I: finite element modeling and validation. Journal of Structural Engineering, ASCE, **132**(1): 13–22. doi:10.1061/(ASCE)0733-9445(2006)132:1(13).

Frangi, A., and Fontana, M. 2003. Elasto-plastic model for timber-concrete composite beams with ductile connection. Structural Engineering International, **13**(1): 47–57. doi:10.2749/101686603777964856.

Gentile, C. 2000. Flexural strengthening of timber bridge beams using FRP. M.A.Sc. dissertation, University of Manitoba, Winnipeg, Man.

Gerber, A. 2016. Timber-concrete composite connectors in flat-plate engineered wood products. MASc. dissertation, University of British Columbia, Vancouver, BC.

Glos, P. 1978. Reliability theory for timber structures: determination of compression strength behaviour of glulam components from interaction of material properties. Heft 34/1978. Laboratorium fuer den Konstruktiven Ingenieurbau, Technische Universitaet Muenchen. (In German)

Hankinson, R.L. 1921. Investigation of crushing strength of spruce at varying angles of grain. Air Service Information Circular, No. 259. U.S. Air Service.

Hashin, Z. 1980. Failure criteria for unidirectional fiber composites. Journal of Applied Mechanics, **47**: 329–333. doi:10.1115/1.3153664.

Hill, R. 1948. A theory of the yielding and plastic flow of anisotropic metals. Proceedings of the Royal Society A, Mathematical, Physical and Engineering Sciences, **193**. doi:10.1098/rspa.1948.0045.

Hoffman, O. 1967. The brittle strength of orthotropic materials. Journal of Composite Materials, **1**: 200–206. doi:10.1177/002199836700100210.

Holmberg, S., Persson, K., and Petersson, H. 1999. Nonlinear mechanical behaviour and analysis of wood and fibre materials. Computers & Structures, **72**(4–5): 459–480. doi:10.1016/S0045-7949(98)00331-9.

Kim, S.-W., and Vecchio, F.J. 2008. Modeling of shear-critical reinforced concrete structures repaired with fiber-reinforced polymer composites. Journal of Structural Engineering, ASCE, **134**(8): 1288–1299. doi:10.1061/(ASCE)0733-9445(2008)134:8(1288).

Liu, C. 2016. Modelling of timber-concrete composite structures subjected to short-term monotonic loading. M.A.Sc. dissertation, University of Toronto, Toronto, Ont.

Le Roy, R., Pham, H.S., and Foret, G. 2009. New wood composite bridges. European Journal of Environmental and Civil Engineering, **13**(9): 1125–1139. doi:10.1080/19648189.2009.9693178.

Neely, S.T. 1899. Relation of compression-endwise to breaking load of beam. Progress in Timber Physics. USDA Division of Forest Circular 18. pp. 13–17.

Norris, C.B. 1950. Strength of orthotropic materials subjected to combined stress. Report No. 18126. U.S. Department of Agriculture, Forest Products Laboratory.

Palermo, D., and Vecchio, F.J. 2004. Compression field modeling of reinforced concrete subjected to reversed loading: verification. Structural Journal, **101**(2): 155–164.

Persaud, R., and Symons, D. 2006. Design and testing of a composite timber and concrete floor system. The Structural Engineer, **21**: 22–30.

Saatci, S., and Vecchio, F.J. 2009. Nonlinear finite element modeling of reinforced concrete structures under impact loads. Structural Journal, **106**(5): 717–725.

Sagbas, G., Vecchio, F.J., and Christopoulos, C. 2011. Computational modeling of the seismic performance of beam-column subassemblies. Journal of Earthquake Engineering, **15**(4): 640–663. doi:10.1080/13632469.2010.508963.

Suseyto, J., Gauvreau, P., and Vecchio, F.J. 2013. Steel fiber-reinforced concrete panels in shear: analysis and modeling. Structural Journal, **110**(2): 285–296.

Van der Linden, M. 1999. Timber-concrete composite beams. Heron, **44**(3): 215–239.

Vecchio, F.J. 2000. Disturbed stress field model for reinforced concrete: formulation. Journal of Structural Engineering, ASCE, **126**(9): 1071–1077. doi:10.1061/(ASCE)0733-9445(2000)126:9(1070).

Vecchio, F.J., and Collins, M.P. 1986. The modified compression field theory for reinforced concrete elements subjected to shear. ACI Journal, **83**(2): 219–231.

VTAG. 2019. Nonlinear finite element analysis software for reinforced concrete structures [home page]. VecTor Analysis Group (VTAG). Available from vectoranalysisgroup.com.

Wong, P.S., Vecchio, F.J., and Trommels, H. 2013. VecTor2 and FormWorks User's Manual. Technical report. Department of Civil Engineering, University of Toronto, Toronto, Ont.

Yeoh, D. 2010. Behaviour and design of timber-concrete composite floor system. Ph.D. dissertation, University of Canterbury, Christchurch, NZ.

Yeoh, D., Fragiacomo, M., De Franceschi, M., and Boon, K.H. 2011. State of the art on timber-concrete composite structures: literature review. Journal of Structural Engineering, ASCE, **137**(10): 1085–1095. doi:10.1061/(ASCE)ST.1943-541X.0000353.

Zhang, C., and Gauvreau, P. 2015. Timber-concrete composite systems with ductile connections. Journal of Structural Engineering, ASCE, **141**(7). doi:10.1061/(ASCE)ST.1943-541X.0001144.